An assessment of the problem of stray light in the optics of the International X-ray Observatory

Frank Spaan*, Richard Willingale
University of Leicester, University Road, Leicester LE1 7RH, United Kingdom

ABSTRACT

Different optical designs are under consideration for the International X-ray Observatory (IXO). In this paper we show results of simulations of the segmented shell Wolter-I design, of the Silicon Pore Optics (SPO) conical Wolter-I approximation and of the Silicon based Kirkpatrick-Baez design. We focus particularly on the issue of stray light. When a source is off axis, such that it is not imaged on the detector, some of its light may still be directed by the optics onto the detector plane. Sources close to the pointing direction can thereby introduce an extra background radiation level in the detectors. This phenomenon is investigated by numerical ray tracing of the three designs, yielding detector images of the stray light, and an indication of which part of the mirror that light originates. Results show the similarities and differences of the designs with respect to stray light, and give a quantitative indication of the level of background radiation in different cases. Furthermore, for the Silicon Pore Optics design, two different ways of partially blocking the stray light have been modelled, indicating that a reduction of the stray light can be achieved. In general, the results that have been found indicate that for the simulated set-ups the stray light levels are compliant with the design specifications of the International X-ray Observatory.

Keywords: **Keywords:** X-ray telescope mirror, Wolter-I, Silicon pore optics, stray light

1. INTRODUCTION

The International X-ray Observatory[1] is being developed as a next space based astronomical telescope for observations at energies from 0.1 to 40 keV, to follow up current observatories like the X-ray Multi-Mirror[2] (XMM-Newton) and Chandra Xray Observatory[3]. The optical design for the International X-ray Observatory is subject of research in Japan, the United States and Europe from which mainly two options have emerged, both based on the classical Wolter-1 design[4].

One option uses a set of segmented glass shells to form a basis for the two parabolic and hyperbolic grazing incidence mirrors. The other option approximates such optics using ribbed Silicon plates without curvature in the axial direction, thereby forming many small pores reflecting the X-rays[5]. For comparison, a third optical system, based on the Kirkpatrick-Baez design[6], is also evaluated.

Because of their fundamental design properties, all three systems will cast light onto the detector, also from sources outside the field of view. This is the case when single reflections occur, instead of the normal two reflections for a ray that is focused within the field of view. Compared to the focused sources inside the field of view, it is a small fraction and is referred to as stray light.

The work described in this paper estimates the amount of stray light and its density spread on the detector for the optical design options of the International X-ray Observatory through numerical ray tracing using purpose written code.

In section 2 we describe the simulations: first the general set-up, then the stray light behavior, in two energies, followed by results on the distribution of the stray light on the detector and possible counter measures; and we end with a discussion.

*fs78@le.ac.uk; phone: +44-116-252-3874; fax: +44-116-252-2464

Space Telescopes and Instrumentation 2010: Ultraviolet to Gamma Ray,
edited by Monique Arnaud, Stephen S. Murray, Tadayuki Takahashi, Proc. of SPIE Vol. 7732,
773240 · © 2010 SPIE · CCC code: 0277-786X/10/$18 · doi: 10.1117/12.857021

2. SIMULATIONS

2.1 General remarks

A ray tracing program, written in Mathematica, was used to assess the effect of stray light. Three optical systems were implemented: the segmented glass shell Wolter-1 configuration (referred to as type 3, for historical reasons), the Silicon pore approximation to the Wolter-1 (type 1) and a Kirkpatrick-Baez system, based on Silicon plates (type 2). We assumed a detector area similar to that of the Wide Field Imager; which has been simulated as a circular field with a radius of 9 arcmin.

It should be noted that the rays that are simulated are generated inside the open pupil area only. However, the amount of optically unused area in a mirror (entrance pupil) is different for each optical type. As the results generally show the efficiency relative to the open pupil area for each type, the difference in starting area usually does not show up. In these simulations, the open pupil areas are 4.15, 5.24 and 7.34 m^2 for types 1, 2 and 3, respectively. Most of the stray light intensities shown hereafter are given as fractions of the total flux entering the open pupil area. This makes comparison of the stray light performance of the three systems easier.

The simulations were run over 10 source angles, 2 energies and with or without stray light counter measures. The source angle values ranged from 0 (on axis) to 180 arcmin; beyond this, the amount of stray light vanishes. We have not taken into account scattering due to roughness of the reflective surface. The general (fixed) parameters used in the simulations are shown in Table 1.

PARAMETER	VALUE	UNIT
Focal length	20	m
Outer mirror radius	1.90	m
Inner mirror radius	0.25	m
Reflective material	Ir	
Surface roughness	0	nm
Support thickness azimuthally (type 1)	16.8	mm
Support thickness radially (type 1)	2	mm
Support thickness for petals (type 1)	70	mm
Si-pore size azimuthally (type 1)	605	μm
Si-pore size radially (type 1 & 2)	605	μm
Number of Si plates per module (type 1 & 2)	45	
Si plate thickness (type 1 & 2)	170	μm
Si-pore size azimuthally (type 2)	100	mm
Support thickness (type 3)	34	mm
Parabola length (type 3)	0.200	m
Glass thickness (type 3)	300	μm
Source orientation	π/8	rad
Resulting calculation precision (in Mathematica)	> 20	digits

Table 1 The general parameters used in the simulations

A type 1 optical module has two parts to effect the double reflection of the Wolter design. Each part consists of a set of Silicon plates which have been polished, ribbed and stacked. In this way many narrow pores are formed, and each of them acts as a reflective optical element, with only one of the four surfaces of each pore being reflective. Each plate is curved in the azimuthal direction, but not in the axial direction. The modules are arranged in 8 petals; the total number of pores is of the order of 10^7.

In the type 2 optics the Silicon plates are not ribbed and the two stacks in the module are oriented perpendicular to each other, thereby effecting the Kirkpatrick-Baez design. The modules are arranged in a sunflower-like spiral[7], which has been shown to have the closest possible packing in this situation. The modules of this type are very similar to each other.

The type 3 optics uses proper para- and hyperbolic surfaces, which are mounted in large modules making up the full Wolter design.

In all designs, the mounting and support structures influence the total effective area of the optic. The structures chosen for these simulations are not optimized, but also do not influence the comparison of the systems very much due to the way the results are prepared, as discussed previously.

In Figure 1, the mirror configurations of the three optical types are shown. On the left the modular arrangement of the Silicon pore optics, in the centre the sunflower arrangement of the square modules of the Kirkpatrick-Baez design, and on the right the segmentation used in the classical glass based Wolter-1 design. In Figure 2 the different reflective surfaces are illustrated, for type 1, 2 and 3, respectively.

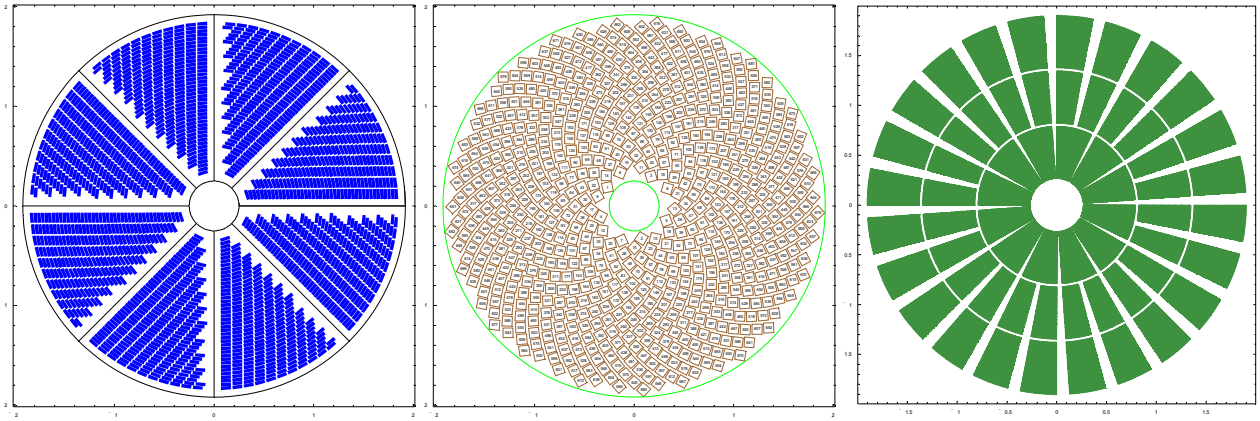

Figure 1 The layout, as used in the simulations, of the optical modules in the mirror plane for: the Silicon pore Wolter-1 optic (left, referred to as type 1 for historical reasons), the Kirkpatrick-Baez optic (centre, type 2) and the segmented Wolter-1 optic (right, type 3).

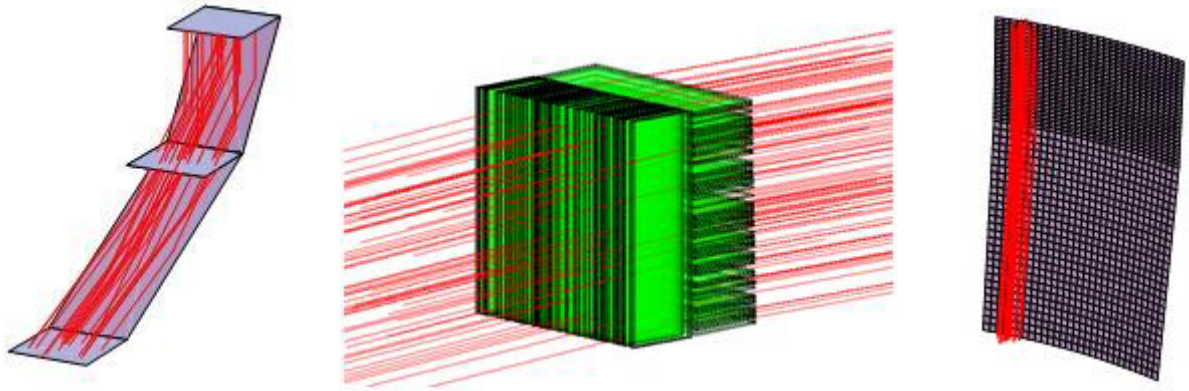

Figure 2 An illustration of the reflective surfaces of the different optics (rays shown in red): left a Silicon pore of type 1, in the centre a set of perpendicular Silicon plates for type 2, and on the right a para-/hyperbolic segment of type 3 (the reflective surfaces are shown using a fine graphics mesh grid). These illustrations have different scales.

2.2 Ray tracing of stray light.

We simulated a point source at different off axis angles, all of which are larger than the field of view; this means that these sources are not focused onto the detector. There are many rays, however, which are not obscured and make it to the detector plane. In Figure 3 are shown, as an example, the hits in the detector plane for a source at an angle of 100 arcmin (10 times the field of view) for each optical type. Each ray that hits the detector plane is shown as a black dot, and the ray-hits that are inside the detector area (which is shown as a (blue) circle) are shown as little (red) circles. Note that the type 1 and 3 systems image the source in the upper right quadrant, the type 2 in the lower left quadrant; this is according to the physical situation. We see a large difference in the number of rays making it through the optical system onto the detector plane, but the number of rays within the detector area differ less between the systems. The number of rays simulated for each point source position and parameter setting was 10^5.

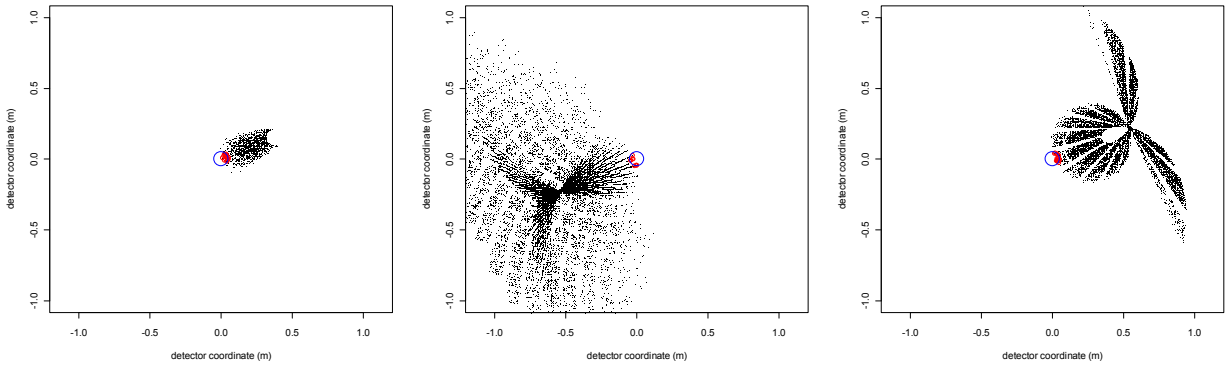

Figure 3 The detector plane, with the position of rays hitting the plane shown as (black) points; within the Wide Field Imager area they are shown as (red) circles. The detector area is shown as a (blue) circle. The point source was at 100 arcmin off axis; shown are the type 1, 2 and 3 optics, from left to right.

In fact, looking at Figure 3 only, the beam seems to be poorly focused, but viewed as a logarithmic three dimensional intensity plot it is clear that there is still a high peak at the point where the source should be focused. This is shown in Figure 4. Note the difference in peak intensity between the three systems; the logarithmic intensity shown here is calculated as the sum of the rays for each positional bin, and taking into account the reflectivity efficiency.

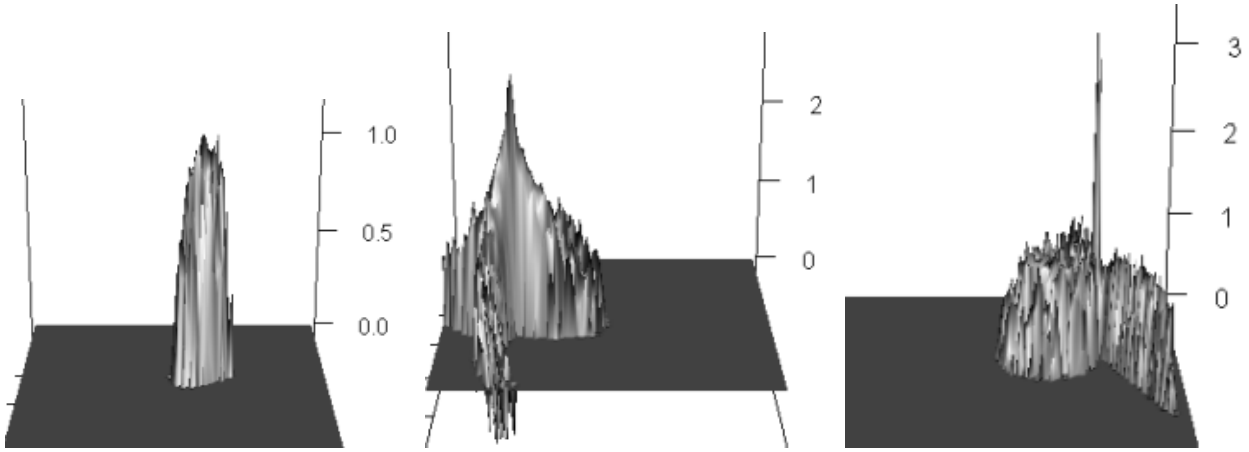

Figure 4 As Figure 3, but now shown in three dimensions with the height as the intensity; note that the height scale is logarithmic and different for each subplot.

2.3 Full stray light detector intensity and grasp

The overall intensity on the detector was calculated by summing the rays in that area, after correction for the reflectivity of each ray at each reflection. This intensity can be calculated for each different source angle and for each of the optical

types. The result is shown in Figure 5, with the intensity shown as the fraction of the total flux in the open pupil area (10^5).

The position of the peak intensity of type 3 is apparently at a smaller angle than with type 1 or 2. This is due to the chosen module constellation which allows for the type 3 modules to be closer to the inner radius of the mirror. The smallest radius used is for type 1 about 33 cm, while for type 3 this is 26 cm. A type 3 constellation with 7 cm wider inner radius does indeed yield no stray rays in the Wide Field Imager area for a source at 20 arcmin, just like for type 1 and 2. This implies that the stray light performance of any of the three constellations is sensitive to the radial position of the innermost refelective surface.

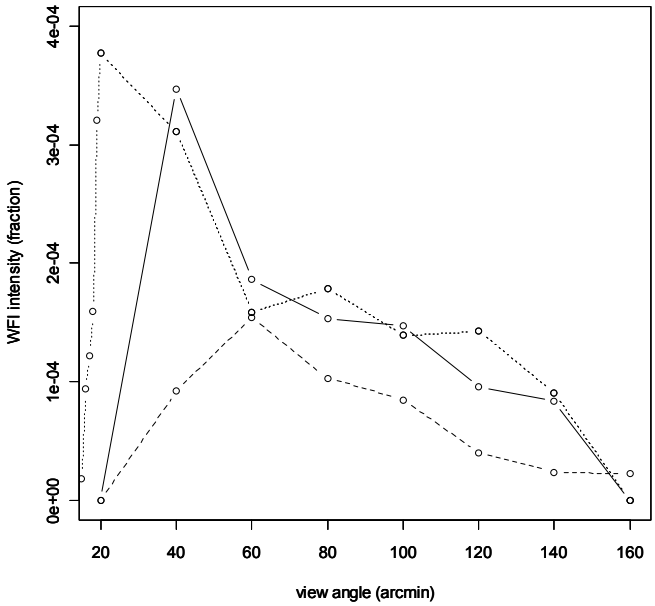

Figure 5 The overall fractional intensity on the Wide Field Imager detector area as a function of the off axis source distance in arcmin for the type 1, 2 and 3 optics (solid, dashed, dotted).

The results shown in Figure 5 can be used to calculate the total intensity of the X-ray sky cast onto the detector as stray light and appearing as detector background radiation. For this we sum over the source angles and sky orientation and obtain this way the grasp using

$$grasp = \int_0^{2\pi} \int_0^{\infty} intensity(r)\, r\, dr\, d\varphi = 2\pi \sum_{i=1}^{N_\alpha} intensity[i] r[i] \Delta r$$

The results for each type are shown in Table 2. The intensity outside the region shown in the plots is assumed to be zero. It should be noted that the value of the grasp depends strongly on other parameters too, like the size of the detector area and the orientation of the point source used with respect to the mirror, due to obscuration at the support structure. In square brackets, the relative values are given with respect to the grasp for a source within the field of view (respectively 506.63, 522.23 and 1051.21 $m^2 arcmin^2$ for 1.25 keV and 90.15, 61.81 and 224.64 for 6 keV).

GRASP ($m^2 arcmin^2$) [% of on axis grasp]	Type 1	Type 2	Type 3
1250 eV	39.27 [7.8%]	29.81 [5.7%]	80.81 [7.7%]
6000 eV	14.91 [16.5%]	12.89 [20.9%]	30.81 [13.7%]

Table 2 The stray light grasp; note that the values which are not in square brackets also depend on the open pupil area that was simulated, and this is different for each type.

The simulations as have been carried out for 1.25 and 6 keV. The results for 6 keV are the same as for 1.25 in terms of the ray positions in the mirror and on the detector, but because the efficiency of the reflection diminishes non-linearly for higher energies, the results differ from the lower energy case; some of the outer mirrors are virtually inactive in forming the point spread function because the reflection angle is so high that at this energy there is no reflection. The main changes are in the grasp; this has been shown in Table 2.

The origin of the stray rays in the mirror can be illustrated by images showing where in the entrance pupil the rays come from that make it to the detector plane. This is shown for each type in Figure 6, again for the same off axis angle of 100 arcmin.

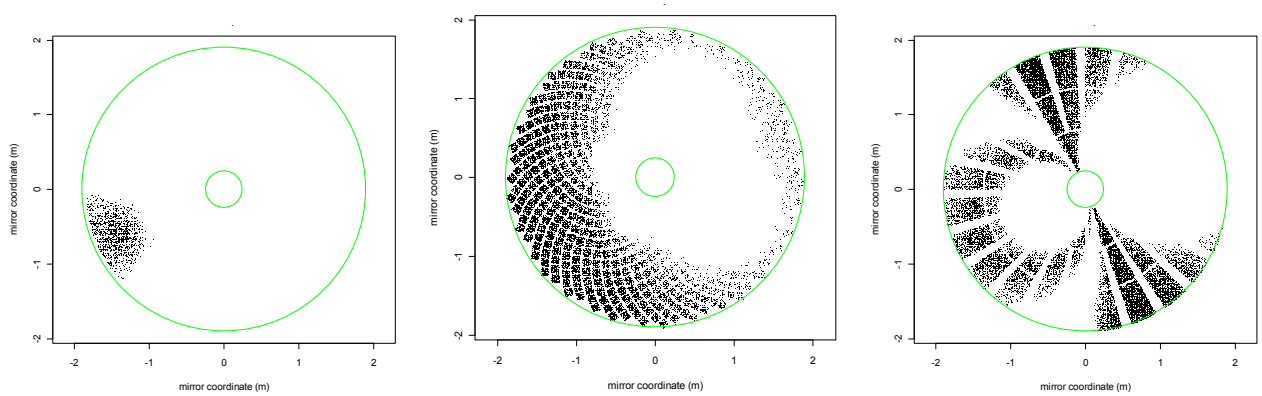

Figure 6 The position in the mirror of any rays that are reflected onto the detector plane for the three optical types (1, 2 and 3 from left to right).

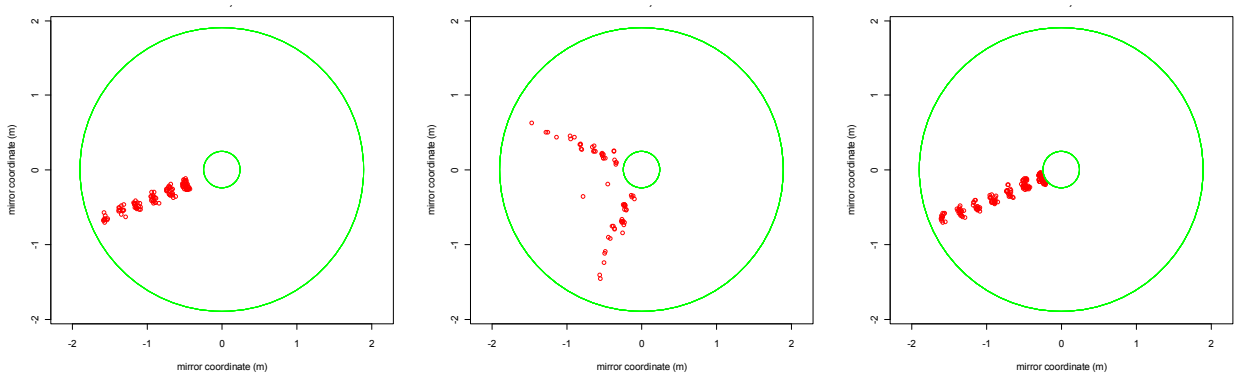

Figure 7 As Figure 6, but now only for the rays that hit the Wide Field Imager area (type 1, 2, 3 from left to right). Each ray position is shown as a (red) circle.

In Figure 7 is shown where in the mirror the rays come from that make it even onto the Wide Field Imager, now for all simulated off axis sources angles combined in one plot for each type. Because there are not many rays, each origin position is indicated with a (red) circle. The rays come only from a narrow band at the source orientation angle ($\pi/8$); for the type 2 system, Kirkpatrick Baez, the two possible single reflections at the perpendicular oriented reflective surfaces is clear (Figure 7, centre).

2.4 The structure of the stray light within the detector area

The stray light on the detector is not distributed uniformly. The following results therefore show the radial structure of the stray light within the Wide Field Imager area. They indicate that the stray light increases with radial distance from the detector centre, being practically zero in the centre. See Figure 8.

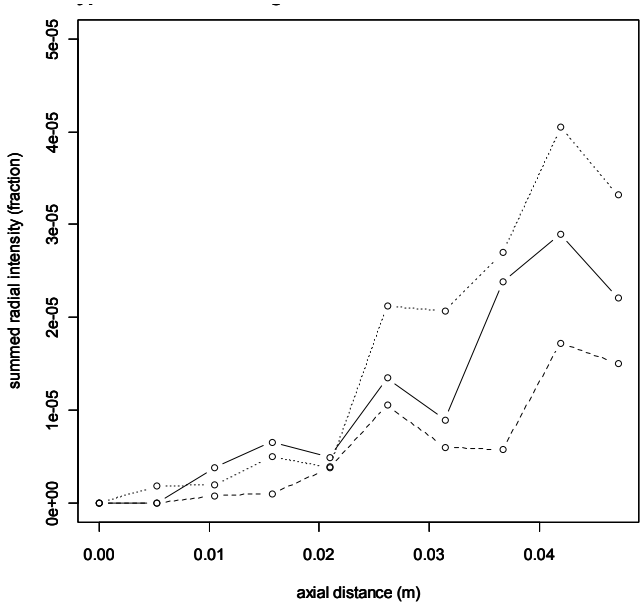

Figure 8 The radial point spread function within the Wide Field Imager area for types 1, 2 and 3: solid, dashed and dotted, respectively. For each type, the intensities of the stray light of all point sources have been summed.

2.5 The influence of stray light counter measures for type 1.

For the Silicon Pore Optics (type 1), two stray light counter measures were simulated:

1) an extension of each plate in the source direction, at an angle equal to the field of view, with an absorbing surface and sharp edge;

2) an intrusion inside the pores, blocking the area which is not traversed by on-axis rays.

An illustration of the principle of the two counter measures is shown in Figure 9. The internal obstruction intrudes the pore by half the radial pore width. The length of the external plate extension is determined by the plate thickness and the angle of the extension which is cut out of the Silicon plate on both sides.

In order to simulate these counter measures, the Silicon pores were now described in the software as flat instead of curved – this is not the same as the proper Silicon pore approximation of the Wolter-1 system as simulated before, which has plates with a curvature in the azimuthal direction leading to a better point spread function. The coordinates of the hits on the detector are slightly different therefore, as they now have an additional azimuthal spread of about 0.6 mm (the azimuthal size of the now not focusing pore) – this is insignificant for the testing of stray light.

The type 2 and 3 systems have not been simulated with stray light counter measures.

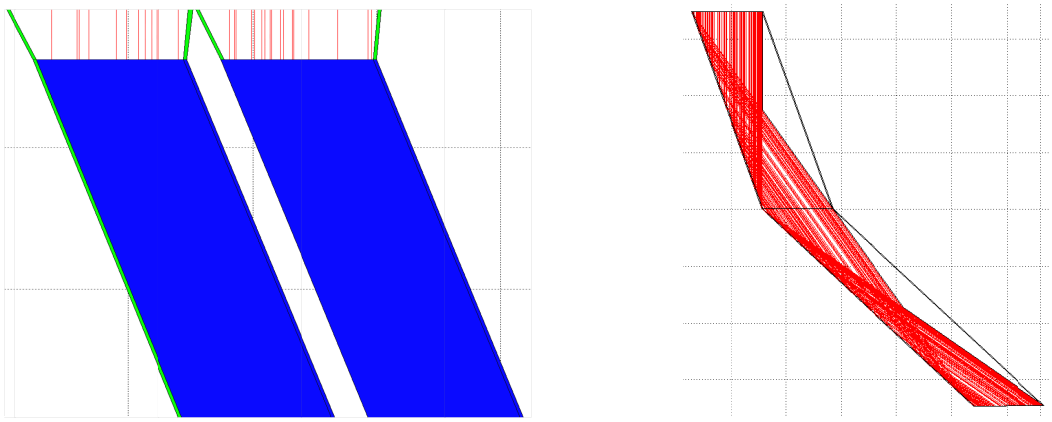

Figure 9 An illustration of the two counter measures that were simulated. Left is shown the cross-section of a part of two pores as solid (blue), with on-axis rays incident from above and the Silicon plate area in between them extended beyond the pore area and shaped to form a small baffle. On the right a cross-section through one pore showing the area which is traversed by on-axis rays; this empty area is filled with Silicon as a second stray light counter measure.

The results are shown in Figure 10 and Table 3. We see an improvement in the stray light performance, especially for the stray light spread on the detector when both stray light blocking counter measures are used.

GRASP (m^2arcmin^2) [% of normal grasp]	without blocking	with internal blocking only	with external blocking only	with both internal and external blocking
	39.27 [100%]	20.93 [53 %]	6.11 [16 %]	1.32 [3 %]

Table 3

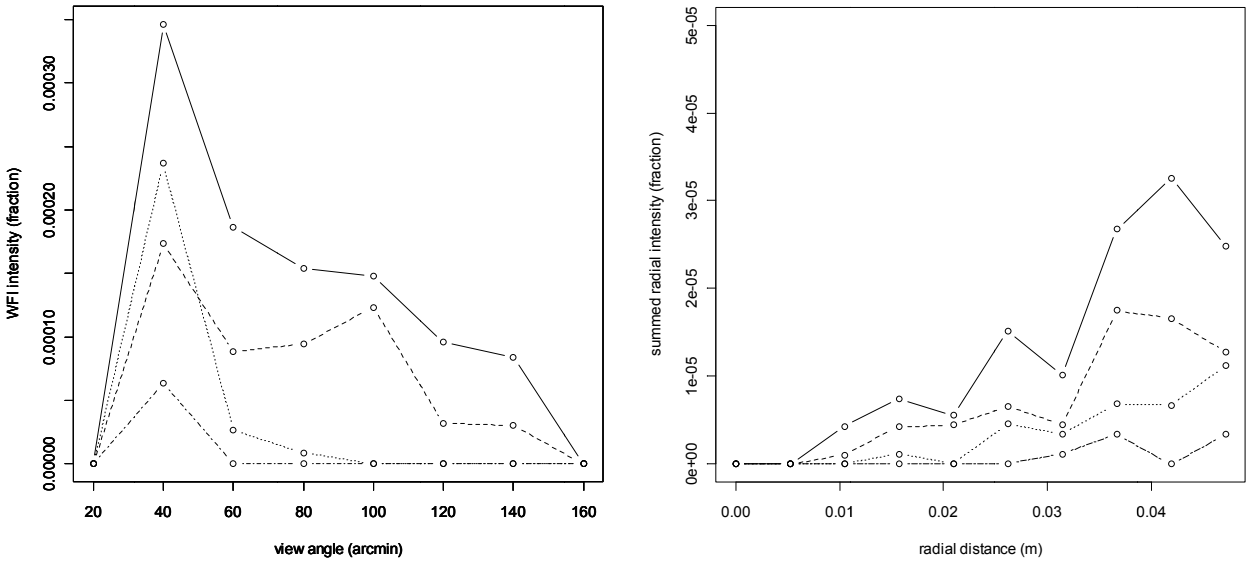

Figure 10 Left: The overall intensity on the detector as a function of the source angle using the stray light counter measures for type 1: without blocking (solid), with internal blocking only (dashed), with external blocking only (dotted) and with both internal and external blocking (long dashed). Right: the radial distribution on the detector for the same stray light counter measures.

3. DISCUSSION

We have shown results of numerical simulations of stray light for three types of optical designs for the International X-ray Observatory: a Silicon pore conical approximation to Wolter-1 (type 1), a Silicon plate based Kirkpatrick-Baez (type 2) and a segmented glass shell Wolter-1 (type 3). Based on these results we arrive at the following conclusions:

There is no significant difference in stray light behavior between the three systems.

The total grasp of the stray light is for all optical types lower than 8% of the grasp of the field of view for 1.25 keV and lower than 21% for 6 keV.

The stray light is less in the centre of the detector in more or less the same way for the three types, yielding virtually no stray light in the first arcmin field of view.

The stray light counter measures for the type 1 optics that have been simulated can decrease the amount of stray light by more than 95%. Although we have not simulated stray light counter measures for other optical types, we expect that such measures are also there possible and effective. In general we expect the practical implementation of stray light counter measures easier for systems with larger sub-pupils, like type 3 in our set of simulated optical systems.

REFERENCES

[1] White, N. E., Parmar, A., Kunieda, H., Nandra, K., Ohashi, T., Bookbinder, J., "The International X-ray Observatory", Proc. X-ray Astronomy 2009 Present status multi-wavelength approach and future perspectives (2009)

[2] Jansen, F.; Lumb, D.; Altieri, B.; Clavel, J.; Ehle, M.; Erd, C.; Gabriel, C.; Guainazzi, M.; Gondoin, P.; Much, R.; Munoz, R.; Santos, M.; Schartel, N.; Texier, D.; Vacanti, G., "XMM-Newton observatory. I. The spacecraft and operations", Astronomy and Astrophysics, 365, L1-L6 (2001)

[3] Weisskopf, M.C., "The Chandra X-Ray Observatory: An overview", Advances in Space Research, volume 32, Issue 10, Pages 2005-2011, (2003)

[4] Wolter, H., "Spiegelsysteme streifenden Einfalls als abbildende Optiken für Röntgenstrahlen," Annalen der Physik 445, 94-114 (1952).

[5] Beijersbergen, M., Kraft, S., Gunther, R., Mieremet, A. L., Collon, M., Bavdaz, M., Lumb, D. H., and Peacock, A. J., "Silicon pore optics: novel lightweight high-resolution x-ray optics developed for XEUS," Proceedings of SPIE 5488, 868 (2004).

[6] Kirkpatrick, P. and Baez, A.V.,"Formation of Optical Images by X-Rays", J. Opt. Soc. Am., 38, 766-773 (1948)

[7] Vogel, H., "A Better Way to Construct the Sunflower Head", Mathematical Biosciences, 44, 179-189 (1979).